JOURNAL OF SOLID STATE CHEMISTRY 47, 6–15 (1983)

Structural Chemistry of Magnéli Phases Ti_nO_{2n-1} ($4 \leq n \leq 9$). III. Valence Ordering of Titanium in Ti_6O_{11} at 130 K*

Y. LE PAGE AND PIERRE STROBEL†

Solid State Chemistry, National Research Council of Canada, Ottawa K1A 0R9, Canada

Received June 28, 1982; and in revised form September 23, 1982

The phase transition at 147 K in Ti_6O_{11} corresponds to the occurrence of a superstructure with tripling of the cell volume on cooling. Its reduced cell parameters at 130 ± 5 K are $a = 7.517(1)$, $b = 11.986(2)$, $c = 13.397(2)$ Å, $\alpha = 98.29(1)$, $\beta = 105.52(1)$, and $\gamma = 107.79(1)$ degrees in space Group $P\bar{1}$ with $Z = 6$. A systematic nomenclature adding one index to the substructure atom names permits calculation of the model's atomic coordinates in the asymmetric unit in terms of the rutile sub-substructure and keeps track of the structural changes. The superstructure was solved by direct methods and refined to $R_F = 5.2\%$ on 3062 observed reflections assuming isotropic thermal motion. A complex pattern of Ti–O and Ti–Ti distance changes is observed. It is interpreted to correspond to valence ordering of the Ti atoms, probably complete in the shear-plane slab and partial in the rutile-like slab. The Ti–Ti distances, with one very short approach of 2.65 Å at a shared face, seem to be consistent with "bipolarons" but can also be analyzed in terms of electrostatic repulsion which allows for the considerable lengthening of some distances as well.

Introduction

Transitions showing up as discontinuities in electrical conductivity and magnetic susceptibility are known to occur in the homologous series of compounds Ti_nO_{2n-1}, $4 \leq n \leq 9$ (1, 2). In Ti_4O_7 (*3*) and Ti_5O_9 (*4*) they correspond to structural changes. Following the growth of millimeter-size crystals of Ti_6O_{11} (*5*) and the refinement of its room-temperature structure (*6*), a low-temperature study of the structure of this compound was undertaken.

Both the Bragg angles and the intensities of a selection of room-temperature high-angle reflections show two discontinuities in the range 95–300 K, corresponding to two discontinuities in the conductance observed at 119 and 147 K (*7*). The present contribution is concerned with the crystal structure of Ti_6O_{11} in the intermediate phase between the two transition temperatures, namely at 130 ± 5 K.

Cell Parameters and Intensity Measurement

The subscript RT indicates the room-temperature cell in (*3, 4*). Oscillation patterns about $[100]_{RT}$ and $[010]_{RT}$ performed at 130 K with graphite-monochromatized Mo$K\alpha$ radiation disclosed two weak layers of reflections between layers expected to be adjacent from the RT cell parameters, indicating the tripling of the periods along these directions. No extra layer could be seen on similar patterns about $[110]_{RT}$ and $[1\bar{1}1]_{RT}$. Preliminary intensity measurement with

* Issued as NRC 20944.

† Present address: Laboratoire de Cristallographie, CNRS, 166X, 38042 Grenoble Cedex, France.

0022-4596/83/040006-10$03.00/0

cell parameters $[\mathbf{a} + \mathbf{b}, 3\mathbf{b}, (\mathbf{a} - \mathbf{b} + \mathbf{c})/2]_{RT}$ showed the corresponding lattice to be primitive. Its primitive reduced (PR) cell based on the three shortest translations and obtuse angles has $[\mathbf{a}, \mathbf{b}, \mathbf{c}]_{PR} = [-(\mathbf{a} + \mathbf{b}), (7\mathbf{a} + 3\mathbf{b} - \mathbf{c})/2, (-\mathbf{a} - 3\mathbf{b} + \mathbf{c})/2]_{RT}$. The corresponding numerical values are summarized in Table I. The intensity measurement technique is described in (*6*) and the data collection details are given in Table II.

TABLE I

CELL DATA

	RT cell (*6*) 298 K	130 K subcell	Primitive reduced (PR), 130 K
a	5.552(1)	5.546(1)	7.517(1)
b	7.126(1)	7.138(1)	11.986(2)
c (Å)	32.233(6)	32.218(6)	13.397(2)
α	66.94(1)	66.99(1)	98.29(1)
β	57.08(1)	57.06(1)	105.52(1)
γ (°)	108.51(1)	108.57(1)	107.79(1)
S.G.	$I\bar{1}$	$I\bar{1}$	$P\bar{1}$
Z	4	4	6

Subcell-to-cell transformation: $-1,-1,0/3.5,1.5,-0.5/-0.5,-1.5,0.5$

Rutile-to-subcell correspondence: $1,0,-1/-1,-1,-1/0,0,-11$

TABLE II

DATA COLLECTION DETAILS[a]

Same sample as in Ref. (*6*).

Temperature: 130 ± 5 K; maximum $2 - \theta$, 55 degrees with Mo$K\alpha$;

4931 unique measurements, 3062 observed (3 sigmas on I), 1869 unobserved;

Gaussian absorption correction with largest dimension 0.3 mm and $\mu = 64$ cm^{-1}.

Final residuals: $R_F = 5.2\%$, $wR_F = 4.8\%$ on 3062 obs; $R_F = 8\%$ on 1690 observed superstructure reflections with $k + l \neq 3n$.

[a] Full description in Ref. (*6*).

Origin and Nomenclature

The motif of the room-temperature structure involves two centrosymmetrical pseudorutile chain segments which can be distinguished by the relative positions of the face and the three edges shared by the terminal TiO_6 octahedra in each segment. The segment through the origin is called segment 1, while the one passing through the symmetry center at $0,\frac{1}{2},0$ is segment 2. They share faces of TiO_6 octahedra in the $(001)_{RT}$ shear plane to make infinite $[\bar{1}01]_{RT}$ chains (*6*).

The motif of the superstructure may be selected to be three room-temperature motifs corresponding through b_{RT} translations, i.e., 6 pseudorutile chain segments. If no inversion center is present, the origin can be placed arbitrarily. If the superstructure is centrosymmetrical, the origin should be selected on an inversion center which can only occur at places where the substructure allows it, namely the middle of a segment 1 or 2, or between two segments 1 or two segments 2. Since the existence of an inversion center at one of these locations implies the existence of others in the other three types of locations due to the observed periods, it follows that the middle of a chain segment 1 can be selected to be the origin in all the cases, irrespective of the presence or absence of centrosymmetry.

A two-index nomenclature permits the systematic description of the independent atoms at room temperature in terms of the underlying rutile structure in this Magnéli series (*8*). The first index represents an arbitrary numbering of the atoms in the motif of rutile. For Ti atoms it corresponds to the type 1 or 2 of the chain segment containing it. The second index represents the number of c_{rutile} translations applied to it and ranges from 0 to $n/2$, where low numbers correspond to atoms in the rutile-like slabs and high numbers, to atoms in the shear-plane slab. The addition of a third index ranging from 0 to 2 here specifies the number of b_{RT} translations applied to the resulting atom. It, therefore, permits the description of all

the independent atoms in the superstructure, assumed here to be centrosymmetrical. It also permits the calculation of their model coordinates from either the refined RT structure or from the rutile structure using the cell transformation in Table I. This

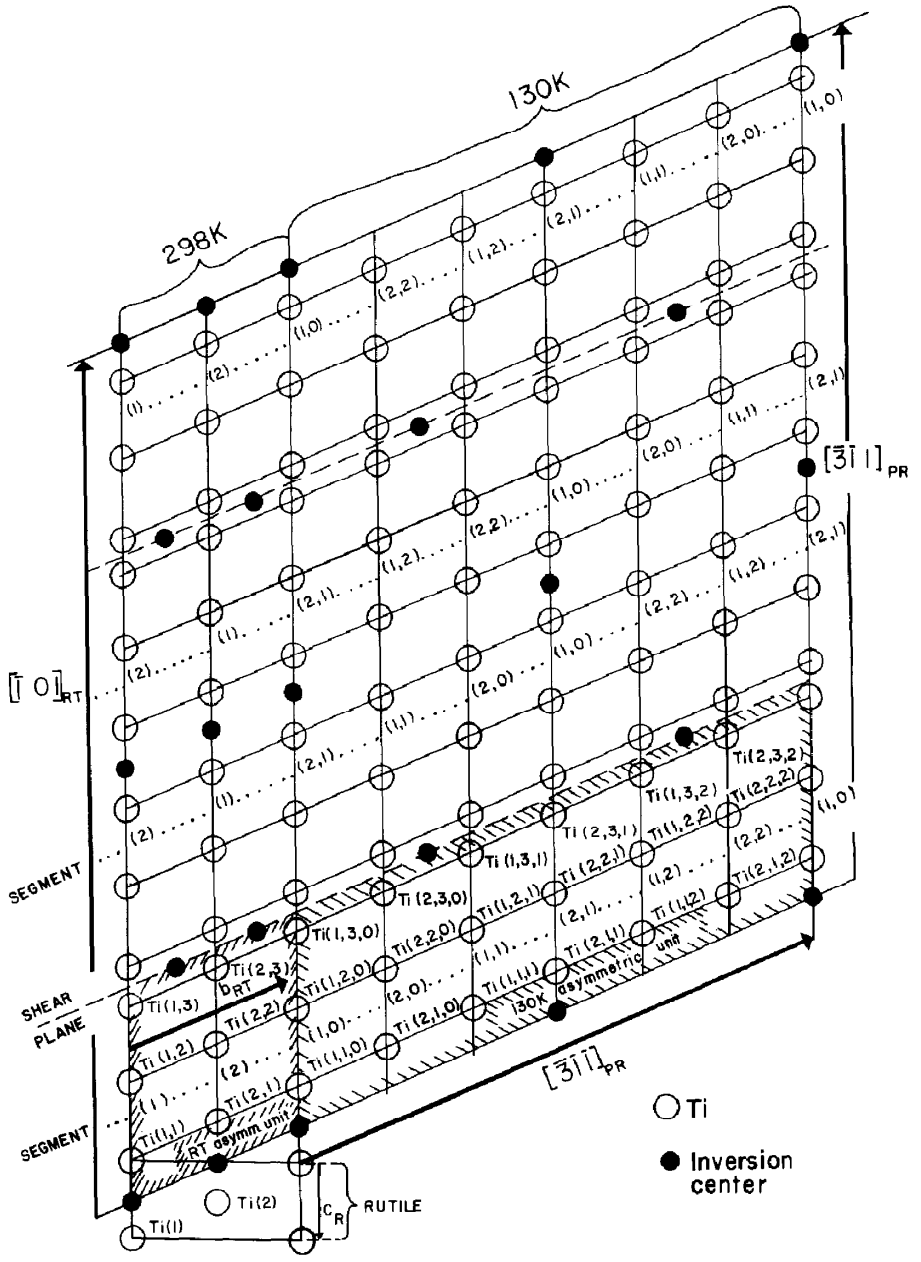

FIG. 1. Projection along $\mathbf{a}_{RT}$ of a slab of the Ti array about the $(101)_{RT}$ plane showing the nomenclature used at 298 and 130 K. It is derived from rutile (R) by addition of indices giving the number of $\mathbf{c}_R$ and $\mathbf{b}_{RT}$ translations applied to a given atom in the motif of rutile (6). The inversion centers shown are in the plane of the figure. Due to the shearing at $\frac{1}{4}$ and $\frac{3}{4}$, the $\mathbf{c}_R$ translation makes a 9.4° angle with its trace in the $(101)_{RT}$ plane and points downwards. The other vectors shown are in the $(101)_{RT}$ plane.

nomenclature is illustrated by the Ti array in the $(101)_{RT}$ plane containing all the edge- and face-sharing in the structure in Fig. 1.

Solution and Refinement of the Superstructure

It seems that superstructures cannot be solved by direct methods due to the absence of large normalized structure factors E among the superstructure reflections. However, the weakness of the superstructure intensities is due to the small amplitude of atomic displacements. If we consider the fictitious structure with same substructure, but where all atomic displacement vectors would be larger by a factor g, the superstructure F values would be larger by approximately the same factor with little change in their phase, while the substructure F values would only be marginally affected in amplitude or in phase. In other words, this fictitious structure is tractable to direct methods provided g is appropriately selected.

Accordingly, after calculating the E values from the measured intensities in the usual way, their values for superstructure reflections were multiplied by a factor 5 while the substructure ones with $k + l = 3n$ were divided by a factor 2. This corresponds to the rescaling of the superstructure intensities by 2 orders of magnitude with respect to the substructure ones. From the input of 25 substructure phases calculated with the above motif and assuming centrosymmetry, the MULTAN program (*9*) proposed a solution with acceptable agreement factors. The E map corresponded to displacements of the Ti atoms. A structure factor calculation with these Ti positions and the model O positions followed by a peak pick on the resulting F_{obs} map permitted initiation of the least-squares refinement of the atomic positions and isotropic thermal parameters using counting statistics weights (Table III).

TABLE III

ATOMIC PARAMETERS X, Y, Z, AND B

	X	Y	Z	B
Ti (1,1,0)	0.13727(22)	0.02810(14)	0.94161(12)	0.340(23)
Ti (1,2,0)	0.42566(21)	0.08682(14)	0.83037(11)	0.281(22)
Ti (1,3,0)	0.29914(21)	0.87112(14)	0.30832(12)	0.275(22)
Ti (2,1,0)	0.36417(21)	0.80428(14)	0.89146(12)	0.358(22)
Ti (2,2,0)	0.07259(21)	0.74813(14)	0.00701(12)	0.328(23)
Ti (2,3,0)	0.19372(21)	0.30203(14)	0.86303(12)	0.278(23)
Ti (1,1,1)	0.13500(21)	0.35851(14)	0.27662(12)	0.299(22)
Ti (1,2,1)	0.43417(21)	0.41556(14)	0.16243(12)	0.295(23)
Ti (1,3,1)	0.30186(21)	0.52800(14)	0.97175(12)	0.330(23)
Ti (2,1,1)	0.36228(22)	0.47360(14)	0.55788(12)	0.359(23)
Ti (2,2,1)	0.07015(21)	0.41260(14)	0.67031(12)	0.324(23)
Ti (2,3,1)	0.19846(21)	0.62583(14)	0.19053(12)	0.291(22)
Ti (1,1,2)	0.14076(21)	0.69396(14)	0.61097(12)	0.323(22)
Ti (1,2,2)	0.43219(21)	0.75299(14)	0.49713(12)	0.287(23)
Ti (1,3,2)	0.30548(21)	0.20666(14)	0.64345(12)	0.241(22)
Ti (2,1,2)	0.35060(21)	0.13546(14)	0.22563(12)	0.339(23)
Ti (2,2,2)	0.06690(21)	0.07884(14)	0.34509(11)	0.259(22)
Ti (2,3,2)	0.19441(21)	0.96193(14)	0.53274(11)	0.233(22)
O (1,1,0)	0.0838(8)	0.7134(5)	0.8646(4)	0.47(9)
O (1,2,0)	0.1993(8)	0.3650(5)	0.0153(5)	0.56(9)
O (2,0,0)	0.3610(8)	0.1046(5)	0.0807(4)	0.41(9)
O (2,1,0)	0.3583(8)	0.8376(5)	0.0391(4)	0.42(9)
O (2,2,0)	0.0971(8)	0.7748(5)	0.1665(4)	0.44(9)
O (3,1,0)	0.0175(8)	0.8912(5)	0.0011(5)	0.62(9)
O (3,2,0)	0.2680(8)	0.1650(5)	0.8836(4)	0.45(9)
O (3,3,0)	0.4557(8)	0.7668(5)	0.2349(4)	0.37(9)
O (4,0,0)	0.3033(8)	0.9540(5)	0.8769(4)	0.53(9)
O (4,1,0)	0.4250(8)	0.9872(5)	0.2459(4)	0.49(9)
O (4,2,0)	0.1716(8)	0.9427(5)	0.3757(4)	0.43(9)
O (1,1,1)	0.0776(8)	0.3784(5)	0.5304(4)	0.57(9)
O (1,2,1)	0.2021(8)	0.6989(5)	0.3419(4)	0.46(9)
O (2,0,1)	0.3574(8)	0.4369(5)	0.4100(4)	0.49(9)
O (2,1,1)	0.3567(8)	0.5063(5)	0.7085(4)	0.50(9)
O (2,2,1)	0.0872(8)	0.4412(5)	0.8302(4)	0.47(9)
O (3,1,1)	0.0163(8)	0.5574(5)	0.6675(5)	0.65(9)
O (3,2,1)	0.2648(8)	0.4970(5)	0.2137(4)	0.49(9)
O (3,3,1)	0.4604(8)	0.4410(5)	0.9018(4)	0.49(9)
O (4,0,1)	0.3015(8)	0.2858(5)	0.2099(4)	0.54(9)
O (4,1,1)	0.4271(8)	0.6580(5)	0.9113(4)	0.42(9)
O (4,2,1)	0.1691(8)	0.6107(5)	0.0455(4)	0.45(9)
O (1,1,2)	0.0800(8)	0.0459(5)	0.1943(4)	0.45(9)
O (1,2,2)	0.2143(8)	0.0416(5)	0.6825(4)	0.48(9)
O (2,0,2)	0.3622(8)	0.7732(5)	0.7466(4)	0.45(9)
O (2,1,2)	0.3619(8)	0.1737(5)	0.3746(4)	0.59(9)
O (2,2,2)	0.1047(8)	0.1092(5)	0.5044(5)	0.52(9)
O (3,1,2)	0.0164(8)	0.2256(5)	0.3331(5)	0.59(9)
O (3,2,2)	0.2664(8)	0.8276(5)	0.5463(4)	0.47(9)
O (3,3,2)	0.4664(8)	0.1084(5)	0.5728(4)	0.50(9)
O (4,0,2)	0.3008(8)	0.6189(5)	0.5406(4)	0.49(9)
O (4,1,2)	0.4257(8)	0.3229(5)	0.5792(4)	0.43(9)
O (4,2,2)	0.1711(8)	0.2777(5)	0.7087(4)	0.45(9)

Note. ESDs refer to the last digit printed.

The final residuals are $R_F = 5.2\%$ and $wR_F = 4.8\%$ on 3062 observed reflections

while $R_F = 8\%$ on the 1690 observed superstructure reflections alone.[1] The relatively high residuals are attributed to the weakness of the superstructure data and to the use of isotropic thermal motion. The mosaic block size of the superstructure as disclosed by the width of its reflections is less than the mosaic block size of the superstructure from the width of its reflections. In other words, more than one superstructure domain exists in a substructure mosaic block where spatial coherence is preserved at all temperatures. Therefore, the basic assumptions of the usual kinematical model of diffraction are not followed; this could also contribute to the residual.

Structure Description and Discussion

The superstructure corresponds to the long-range order of small variations in the Ti–O and Ti–Ti distances (Tables IV and V). Ionic valences for the Ti atoms were calculated using the relationship between the bond length d and the corresponding bond strength s proposed by Zachariasen (*10*):

$$s = e^{(d(1)-d)/B}$$

where $d(1)$ and B are the tabulated lengths 1.823 and 0.324 Å and e is the well-known Euler's constant. A bond length of 1.823 Å would therefore correspond to a bond strength of 1 valence unit (v.u.), while one with length $d(1) + B = 2.147$ Å would correspond to a $1/e$ v.u. strength. The valence of the Ti atom is therefore obtained as the sum of the bond strengths of its bonds with oxygen atoms. This method is more appropriate here than other bond-valence summation methods because the concept of different atomic radii for Ti^{3+} and Ti^{4+} is not required and the valence of Ti is the result of the calculation. The differences between this method and the approximation used previously (*3, 4, 6*) in which the average Ti–O distance determined the valence are slight, at least for sites with little distortion, but it may be up to 0.2 v.u. where the distortion is large.

On the whole, the trend is towards the separation of the valences into three groups with calculated values of approximately 3.85, 3.55, and 3.25. Changes are not pronounced in chain segments of type 1 with the notable exception of the atom Ti(1,3,1), for which the valence drops from 3.70 to 3.30 between 298 and 130 K. On the contrary, the three chain segments derived from the room-temperature segment 2 differ considerably as shown in Fig. 2. In the segment (2,0) which contains the atoms Ti(2,x,0) and in the segment (2,2) the tendency to a highly charged rutile-like region and a less charged shear-plane region observed at 298 K is emphasized at 130 K. The opposite is seen to occur in segment (2,1) where the valences of the terminal atoms increase considerably. Valences close to 4 are observed in the middle of chain segments (2,0), (2,2) as well as near the shear plane in the segments (1,0), (1,2), and (2,1) at 130 K. However, valences close to 3 are observed only in the shear-plane slab. This could be expected from the bond-valence summation on oxygen atoms, some of them having 4 Ti neighbors in the shear-plane slab, while they have only 3 neighbors in the rutile-like slab.

Concurrently, while most Ti–Ti distances are only slightly altered, some of them decrease considerably and others increase considerably (Table VI). It is ob-

[1] See NAPS document No. 04021 for 27 pages of supplementary material. Order from ASIS/NAPS, Microfiche Publications, P.O. Box 3513, Grand Central Station, New York, NY 10163. Remit in advance $4.00 for microfiche copy or for photocopy, $7.75 up to 20 pages plus $.30 for each additional page. All orders must be prepaid. Institutions and organizations may order by purchase order. However, there is a billing and handling charge for this service of $15. Foreign orders add $4.50 for postage and handling, for the first 20 pages, and $1.00 for additional 10 pages of material. Remit $1.50 for postage of any microfiche orders.

TABLE IV

Ti–O Distances

								Room-temp. structure (*6*)	
Ti(1,1,0)–O(1,1,2)	1.956	Ti(1,1,1)–O(1,1,0)	2.006	Ti(1,1,2)–O(1,1,1)	2.006	Ti(1,1)–O(1,1)	1.983
–O(2,0,0)	2.007	–O(2,0,1)	1.957	–O(2,0,2)	1.973	–O(2,0)	1.976
–O(3,1,0)	1.957	–O(3,1,1)	1.952	–O(3,1,2)	1.962	–O(3,1)	1.967
–O(3,2,0)	2.013	–O(3,2,1)	2.067	–O(3,2,2)	2.031	–O(3,2)	2.040
–O(3,1,0)	1.999	–O(3,1,2)	1.936	–O(3,1,1)	1.982	–O(3,1)	1.973
–O(4,0,0)	2.033	–O(4,0,1)	2.041	–O(4,0,2)	2.042	–O(4,0)	2.029
Ti(1,2,0)–O(1,2,2)	2.055	Ti(1,2,1)–O(1,2,0)	2.124	Ti(1,2,2)–O(1,2,1)	2.177	Ti(1,2)–O(1,2)	2.113
–O(2,1,0)	1.908	–O(2,1,1)	1.875	–O(2,1,2)	1.852	–O(2,1)	1.884
–O(3,2,0)	1.931	–O(3,2,1)	2.020	–O(3,2,2)	1.933	–O(3,2)	1.973
–O(3,3,0)	2.132	–O(3,3,1)	2.070	–O(3,3,2)	2.068	–O(3,3)	2.100
–O(4,0,0)	1.862	–O(4,0,1)	1.869	–O(4,0,2)	1.872	–O(4,0)	1.881
–O(4,1,0)	2.013	–O(4,1,1)	1.924	–O(4,1,2)	1.982	–O(4,1)	1.967
Ti(1,3,0)–O(3,3,2)	1.955	Ti(1,3,1)–O(3,3,1)	1.998	Ti(1,3,2)–O(3,3,0)	1.979	Ti(1,3)–O(3,3)	1.971
–O(2,2,0)	2.000	–O(2,2,1)	2.013	–O(2,2,2)	1.976	–O(2,2)	2.000
–O(3,3,0)	2.254	–O(3,3,1)	2.112	–O(3,3,2)	2.216	–O(3,3)	2.199
–O(1,2,1)	2.215	–O(1,2,0)	2.098	–O(1,2,2)	2.078	–O(1,2)	2.118
–O(4,1,0)	1.867	–O(4,1,1)	1.962	–O(4,1,2)	1.868	–O(4,1)	1.884
–O(4,2,0)	1.792	–O(4,2,1)	1.951	–O(4,2,2)	1.815	–O(4,2)	1.842
Ti(2,1,0)–O(2,0,2)	1.918	Ti(2,1,1)–O(2,0,1)	1.943	Ti(2,1,2)–O(2,0,0)	1.951	Ti(2,1)–O(2,0)	1.944
–O(1,1,0)	1.959	–O(1,1,1)	1.996	–O(1,1,2)	1.883	–O(1,1)	1.951
–O(2,0,0)	1.921	–O(2,0,1)	1.954	–O(2,0,2)	2.001	–O(2,0)	1.953
–O(2,1,0)	1.976	–O(2,1,1)	2.014	–O(2,1,2)	1.955	–O(2,1)	1.979
–O(4,0,0)	2.005	–O(4,0,2)	1.963	–O(4,0,1)	1.975	–O(4,0)	1.966
–O(4,1,1)	1.985	–O(4,1,2)	2.042	–O(4,1,0)	2.052	–O(4,1)	2.051
Ti(2,2,0)–O(1,1,0)	1.923	Ti(2,2,1)–O(1,1,1)	1.880	Ti(2,2,2)–O(1,1,2)	2.037	Ti(2,2)–O(1,1)	1.941
–O(1,2,0)	1.992	–O(1,2,1)	2.022	–O(1,2,2)	2.062	–O(1,2)	2.032
–O(2,1,0)	1.978	–O(2,1,1)	1.982	–O(2,1,2)	2.056	–O(2,1)	1.994
–O(2,2,0)	2.063	–O(2,2,1)	2.082	–O(2,2,2)	2.038	–O(2,2)	2.065
–O(3,1,0)	1.890	–O(3,1,1)	1.902	–O(3,1,2)	1.928	–O(3,1)	1.901
–O(4,2,1)	2.069	–O(4,2,2)	2.058	–O(4,2,0)	2.062	–O(3,2)	2.077
Ti(2,3,0)–O(1,2,0)	2.054	Ti(2,3,1)–O(1,2,1)	2.080	Ti(2,3,2)–O(1,2,2)	2.039	Ti(2,3)–O(1,2)	2.046
–O(3,3,1)	2.053	–O(3,3,0)	2.011	–O(3,3,2)	2.121	–O(3,3)	2.059
–O(2,2,0)	1.997	–O(2,2,1)	1.974	–O(2,2,2)	2.034	–O(2,2)	1.993
–O(3,2,0)	1.922	–O(3,2,1)	1.804	–O(3,2,2)	1.866	–O(3,2)	1.847
–O(4,2,2)	1.999	–O(4,2,1)	1.871	–O(4,2,0)	2.038	–O(4,2)	1.961
–O(2,2,1)	2.111	–O(2,2,0)	2.177	–O(2,2,2)	2.122	–O(2,2)	2.149

Note. All sigmas are 0.006 Å except those for room temperature which are 0.003 Å.

served that the Ti atoms whose charge decreases occur in pairs. The corresponding Ti–Ti distance in the $[\bar{1}01]_{RT}$ chains decreases. This fact can be interpreted to correspond to the establishment of a covalent bond between Ti^{3+} neighbors to form a "bipolaron" (*11*), but this does not explain the considerable lengthening of other bonds. The observation of Ti^{3+} pairs at the end of chain segment (2,2) is in line with a similar observation in Ti_4O_7 at 120 K (*3*), also in a segment of type 2. However, the existence of a pair at the face sharing of the octahedra centered on Ti(1,3,1) and Ti(2,3,0) with a very short distance of 2.65 Å to be compared with 2.89 Å in metallic Ti is a remarkable new observation.

The simultaneous valence and distance

TABLE V

IONIC VALENCES FROM BOND-VALENCE SUMMATION ON THE Ti–O BONDS ACCORDING TO (*10*)

130 K						298 K (Ref. (6))	
Ti(1,1,0)	3.55	Ti(1,1,1)	3.59	Ti(1,1,2)	3.50	Ti(1,1)	3.54
Ti(1,2,0)	3.80	Ti(1,2,1)	3.86	Ti(1,2,2)	3.90	Ti(1,2)	3.76
Ti(1,3,0)	3.88	Ti(1,3,1)	3.30	Ti(1,3,2)	3.89	Ti(1,3)	3.70
Ti(2,1,0)	3.94	Ti(2,1,1)	3.66	Ti(2,1,2)	3.87	Ti(2,1)	3.79
Ti(2,2,0)	3.71	Ti(2,2,1)	3.71	Ti(2,2,2)	3.20	Ti(2,2)	3.55
Ti(2,3,0)	3.30	Ti(2,3,1)	3.90	Ti(2,3,2)	3.22	Ti(2,3)	3.52

changes can also be analyzed in terms of electrostatic repulsion. The quantity vv'/r^2 is assumed to be proportional to the repulsion between the atoms Ti and Ti′ with valences v and v' (Table V) separated by the distance r (Table VI). The variation of ionic repulsion $\Delta vv'/r^2$ between 298 and 130 K is plotted vs Δr both for the edge- and face-sharing TiO_6 octahedra in the $[\bar{1}01]_{RT}$ chains (Fig. 3a) and the edge-sharing octahedra between adjacent chains (Fig. 3b). In these plots, a variation of valence only would result in a vertical line at $\Delta r = 0$, while a variation of distance only corresponds to the dotted curve with negative slope in Fig. 3a. If the valence and distance changes were uncorrelated, we would expect to see a scatter of experimental points about these curves, i.e., the experimental points would plot in the second and fourth quadrants essentially. However, the rather long interactions between adjacent $[\bar{1}01]_{RT}$ chains show a considerable range of repulsion with only one chemically significant distance change at the very long edge sharing between

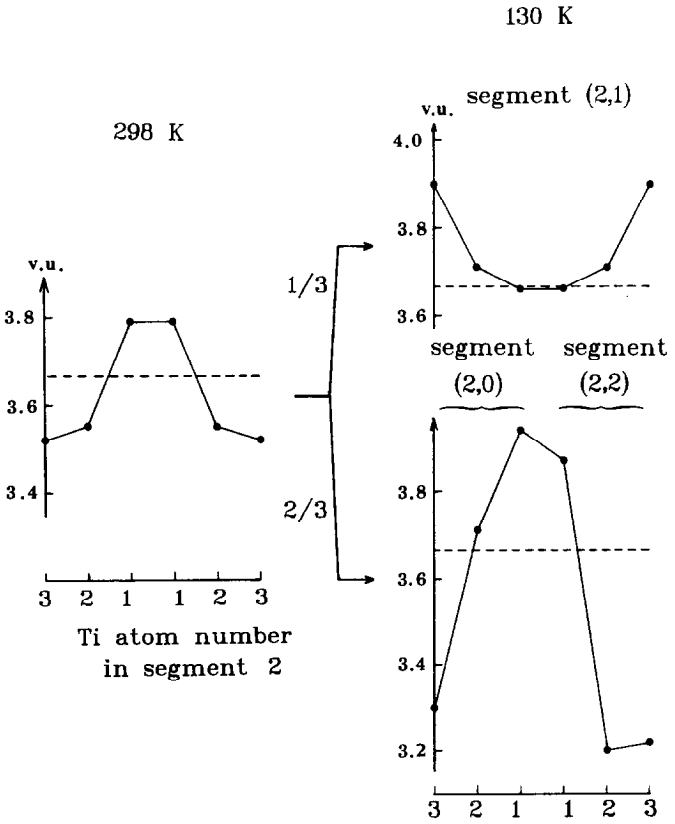

FIG. 2. The evolution of valences in chain segments of type 2 between 298 and 130 K. The dashed line shows the average chemical valence 11/3.

TABLE VI

Ti–Ti Distances at Shared Edges or Faces at 130 K

							Room-Temp. structure (6)
Ti(1,1,0)–Ti(1,1,0)	2.888	Ti(1,1,1)–Ti(1,1,2)	2.847	Ti(1,1,2)–Ti(1,1,1)	2.847	Ti(1,1)–Ti(1,1)	2.878
–Ti(1,2,0)	2.918	–Ti(1,2,1)	3.011	–Ti(1,2,2)	2.963	–Ti(1,2)	2.964
Ti(1,2,0)–Ti(1,1,0)	2.918	Ti(1,2,1)–Ti(1,1,1)	3.011	Ti(1,2,2)–Ti(1,1,2)	2.963	Ti(1,2)–Ti(1,1)	2.964
–Ti(1,3,0)	3.110	–Ti(1,3,1)	3.011	–Ti(1,3,2)	3.056	–Ti(1,3)	3.055
–Ti(1,3,2)	3.126	–Ti(1,3,1)	3.128	–Ti(1,3,0)	3.154	–Ti(1,3)	3.129 *e*
Ti(1,3,0)–Ti(1,2,0)	3.110	Ti(1,3,1)–Ti(1,2,1)	3.011	Ti(1,3,2)–Ti(1,2,2)	3.056	Ti(1,3)–Ti(1,2)	3.055
–Ti(1,2,2)	3.154	–Ti(1,2,1)	3.128	–Ti(1,2,0)	3.126	–Ti(1,2)	3.129 *e*
–Ti(1,3,2)	3.310	–Ti(1,3,1)	3.172	–Ti(1,3,0)	3.310	–Ti(1,3)	3.279 *e*
–Ti(2,3,1)	2.893	–Ti(2,3,0)	2.646	–Ti(2,3,2)	2.844	–Ti(2.3)	2.834 *f*
Ti(2,1,0)–Ti(2,1,2)	2.960	Ti(2,1,1)–Ti(2,1,1)	2.880	Ti(2,1,2)–Ti(2,1,0)	2.960	Ti(2,1)–Ti(2,1)	2.936
–Ti(2,2,0)	2.978	–Ti(2,2,1)	2.955	–Ti(2,2,2)	2.971	–Ti(2,2)	2.960
Ti(2,2,0)–Ti(2,1,0)	2.978	Ti(2,2,1)–Ti(2,1,1)	2.955	Ti(2,2,2)–Ti(2,1,2)	2.971	Ti(2,2)–Ti(2,1)	2.960
–Ti(2,3,0)	2.972	–Ti(2,3,1)	3.075	–Ti(2,3,2)	2.853	–Ti(2,3)	2.973
–Ti(2,3,1)	3.119	–Ti(2,3,0)	3.121	–Ti(2,3,2)	3.122	–Ti(2,3)	3.133 *e*
Ti(2,3,0)–Ti(1,3,1)	2.646	Ti(2,3,1)–Ti(1,3,0)	2.893	Ti(2,3,2)–Ti(1,3,2)	2.844	Ti(2,3)–Ti(1,3)	2.834 *f*
–Ti(2,2,0)	2.972	–Ti(2,2,1)	3.075	–Ti(2,2,2)	2.853	–Ti(2,2)	2.973
–Ti(2,2,1)	3.121	–Ti(2,2,0)	3.119	–Ti(2,2,2)	3.122	–Ti(2,2)	3.133 *e*
–Ti(2,3,1)	3.249	–Ti(2,3,0)	3.249	–Ti(2,3,2)	3.261	–Ti(2,3)	3.261 *e*

Note. All sigmas are 0.002 Å except those for room temperature which are 0.001 Å. *e* indicates an edge shared between adjacent $[\bar{1}01]_{RT}$ chains; *f* indicates a shared face inside a $[\bar{1}01]_{RT}$ chain.

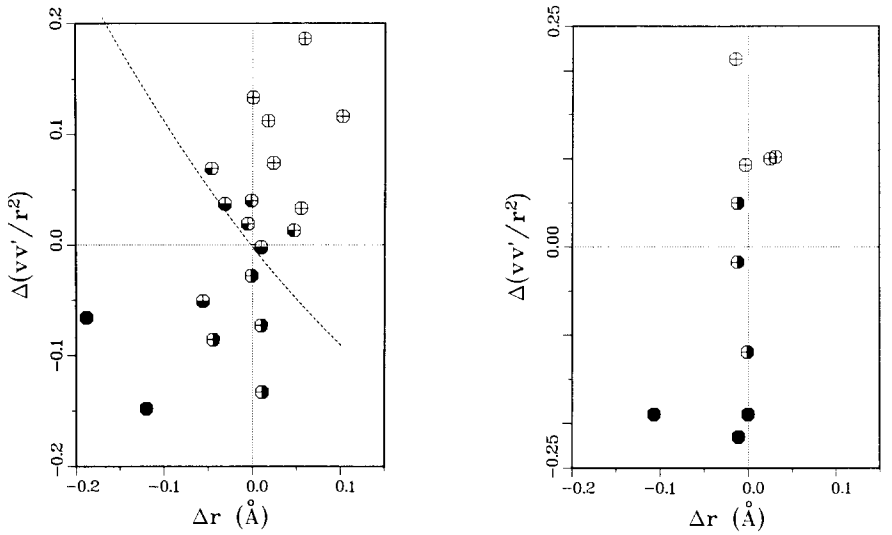

FIG. 3. (a) Change in electrostatic repulsion $\Delta(vv'/r^2)$ vs distance change Δr for Ti neighbors in $[\bar{1}01]_{RT}$ chains from 298 to 130 K with valences from Table V and distances from Table VI. The blackening of the right and left halves of the experimental circles gives the ideal valences of the two Ti atoms at 130 K. The dashed curve corresponds to a distance change without valence change. (b) Same as Fig. 3a, but for edges shared between adjacent $[\bar{1}01]_{RT}$ chains.

Ti(1,3,1) and Ti(1,3,1) of 3.28 Å which shortens to 3.17 Å (Fig. 3b). On the other hand, the distances in the chains plotted on Fig. 3a lie essentially in the first and third quadrants, i.e., shorter Ti–Ti distances correspond to *decreased* repulsions and longer distances to increased repulsions which is unexpected. The complex pattern of observed valence and distance changes can therefore be interpreted as a rearrangement of the Ti–Ti distances that partially compensates the ionic repulsion change, due to the valence change of the Ti atoms.

It is surprising that although this transition is clearly due to the long-range order of valences, the low values of the valences do not scatter about 3+, but rather about 3.25. If we assume that what we observe is a transformation which is only two thirds complete, i.e., all the changes observed are in the correct sense but with only two thirds of the correct amplitude, the valences after the complete transformation would be as shown in Table VII. The valences shown in this table are clearly divided into three classes which can be approximated to 3+, 3.5+, and 4+ within experimental error. We believe that this ideal distribution shown in Fig. 4 is the correct interpretation of our observations. Various reasons for the reduced observed amplitudes could be (a) the transformation occurs gradually and is only two thirds complete at 130 K; (b) the transformation is complete, but the measured diffracted amplitudes are one third too low for superstructure reflections, which may be due to the wider peak profiles, to the above-mentioned violation of the assumptions concerning the kinematical model of diffraction, or to a combination of both. A structural study at several temperatures between 119 and 147 K would throw some light on this point.

No structural interpretation of electrical or magnetic properties was attempted because this will be investigated in forthcoming contributions.

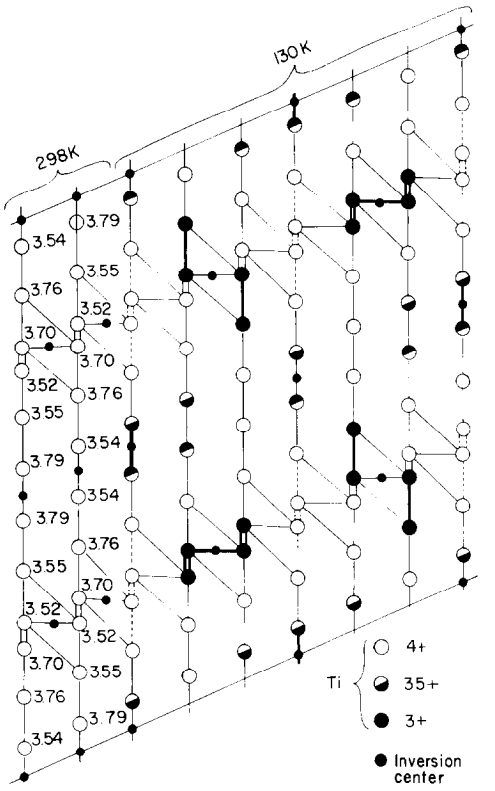

FIG. 4. Ideal distribution of valences from Table VII. It is here assumed that the observed valences as given in Table V correspond to a $\frac{2}{3}$ transformed structure. Single lines between Ti atoms represent a shared edge, double lines a shared face. The distances which were observed to decrease by more than 0.05 Å in Table VI are represented by broader lines, those which increased by more than 0.05 Å are represented by dashed lines. The atom names can be read off Fig. 1.

TABLE VII

IONIC VALENCES FOR A COMPLETE TRANSFORMATION, ASSUMING THAT THE OBSERVED VALUES IN TABLE V CORRESPOND TO A TWO THIRDS COMPLETE TRANSFORMATION

Ti(1,1,0)	3.55	Ti(1,1,1)	3.61	Ti(1,1,2)	3.48
Ti(1,2,0)	3.82	Ti(1,2,1)	3.91	Ti(1,2,2)	3.97
Ti(1,3,0)	3.97	Ti(1,3,1)	3.10	Ti(1,3,2)	3.97
Ti(2,1,0)	4.01	Ti(2,1,1)	3.59	Ti(2,1,2)	3.91
Ti(2,2,0)	3.79	Ti(2,2,1)	3.79	Ti(2,2,2)	3.02
Ti(2,3,0)	3.19	Ti(2,3,1)	4.09	Ti(2,3,2)	3.07

Conclusion

The transition at 147 K in Ti_6O_{11} corresponds to the occurrence of a superstructure on cooling with tripling of the cell volume. The valence ordering, probably complete in the shear-plane slab and partial in the rutile-like slab, is seen to occur. The considerable Ti^{3+}–Ti^{3+} distance reductions observed at the ends of some chain segments of type 2 and at the face sharing might correspond to "bipolarons," but can also be interpreted in terms of ionic repulsion which allows for the considerable lengthening of other distances as well.

Acknowledgments

We thank Dr. L. D. Calvert and Dr. C. M. Hurd for their constant interest in this work.

References

1. R. F. Bartholomew and D. R. Frankl, *Phys. Rev.* **187,** 828 (1969).
2. W. J. Danley and L. N. Mulay, *Mater. Res. Bull.* **7,** 739 (1972).
3. M. Marezio, D. B. McWhan, P. D. Dernier, and J. P. Remeika, *J. Solid State Chem.* **6,** 213 (1973).
4. M. Marezio, D. Tranqui, S. Lakkis, and C. Schlenker, *Phys. Rev. Sect. B* **16,** 2811 (1977).
5. P. Strobel and Y. Le Page, *J. Mater. Sci.* **17,** 2424 (1982).
6. Y. Le Page and P. Strobel, *J. Solid State Chem.* **44,** 273 (1982).
7. A. D. Inglis, P. Strobel, Y. Le Page, and C. M. Hurd, *J. Phys. C. Solid State* (1983), in press.
8. Y. Le Page and P. Strobel, *J. Solid State Chem.* **43,** 314 (1982).
9. G. Germain, P. Main, and M. M. Woolfson, *Acta Crystallogr. Sect. A* **27,** 368 (1971).
10. W. H. Zachariasen, *J. Less-Common Met.* **62,** 1 (1978).
11. S. Lakkis, C. Schlenker, B. K. Chakraverty, and R. Buder, *Phys. Rev. Sect. B* **14,** 1429 (1976).